Polylactide/Montmorillonite Nanocomposites and Microcomposites Prepared by Melt Blending: Structure and Some Physical Properties

M. Pluta,[1] A. Galeski,[1] M. Alexandre,[2] M.-A. Paul,[2] P. Dubois[2]

[1]*Centre of Molecular and Macromolecular Studies, Polish Academy of Sciences, Sienkiewicza 112, 90-363 Lodz, Poland*
[2]*Laboratory of Polymeric and Composite Materials, University of Mons-Hainaut, 20 Place du Parc, B-7000 Mons, Belgium*

Received 25 April 2001; accepted 2 April 2002

ABSTRACT: Polylactide (PLA)/clay nanocomposites loaded with 3 wt % organomodified montmorillonite and PLA/clay microcomposites containing 3 wt % sodium montmorillonite were prepared by melt blending. We investigated the morphology and thermal properties of the nanocomposites and microcomposites and compared them with unfilled PLA, keeping the same thermomechanical history. The influence of the processing temperature on the structural characteristics of the investigated systems was determined. The investigations were performed with differential scanning calorimetry (DSC), thermogravimetric analysis (TGA), X-ray diffraction (XRD), size exclusion chromatography (SEC), and polarized light microscopy (LM). XRD showed that the good affinity between the organomodified clay and the PLA was sufficient to form intercalated structure in the nanocomposite. The microcomposite featured a phase-separated constitution. DSC and LM studies showed that the nature of the filler affected the ordering of the PLA matrix at the molecular and supermolecular levels. According to TGA, the PLA-based nanocomposites exhibited improvement in their thermal stability in air. Reduced flammability, together with char formation, was also observed for nanocomposites, compared to the microcomposites and pure PLA. © 2002 Wiley Periodicals, Inc. J Appl Polym Sci 86: 1497–1506, 2002

Key words: clay; nanocomposites; thermal properties; polylactide

INTRODUCTION

Scientific and industrial interest in polylactide (PLA) has resulted from the beneficial performance of this polymer in terms of physical properties, good processability on standard plastic equipment (extrusion, injection, and film and fiber forming), production from renewable resources (biomass), and biodegradability.[1] This latter feature makes PLA friendly to the environment. Furthermore, the properties of PLA can be modified in a controlled manner by changing its stereochemical structure (in the polymerization stage, i.e., with a mixture of the L or D isomers) and/or by blending it with selected polymers or filling it with inorganic microparticles or nanoparticles.

We aimed in this study to prepare nanocomposites based on PLA by filling it with organically treated clay particles of nanometer-scale and large aspect ratio. Clay-based nanocomposites have already been prepared with a large variety of polymer matrices, including polypropylene,[2] nylon,[3] poly(ethylene terephthalate),[4] polystyrene (PS),[5] unsaturated polyester,[6] polyimide,[7] polyurethane,[8] poly(methyl methacrylate),[9] poly(ethylene oxide),[10] ethylene–vinyl acetate copolymers,[11] and others. Depending on the nature of the polymer, composites can be prepared by different methods, including solution mixing, *in situ* intercalative polymerization, and melt intercalation.[12] The interest in polymer nanocomposites has been inspired by the fact that they usually exhibit improved physical and chemical properties, even at very low clay contents, ranging from 1 to 5 wt %, compared to more classical microcomposites. High enhancements in the fields of mechanical behavior, barrier properties, and thermal stability are believed to result from synergistic interactions between the high surface area of clay galleries and the polymer, combined with the specific constitution of the system because of intercalation and/or exfoliation phenomena.[12]

Correspondence to: M. Pluta (mpluta@bilbo.cbmm.lodz.pl).
Contract grant sponsor: Poland State Committee for Scientific Research; contract grant number: PBZ/KBN-013/T08/39 (the nano part of the work).
Contract grant sponsor: Poland State Committee for Scientific Research; contract grant number: 7 TO8E 027 19 (the PLA part of the work).
Contract grant sponsor: "Région Wallonne" and European Community (FEDER and FSE) in the frame of "Pôle d'Excellence Materia Nova: Objectif 1."
Contract grant sponsor: FRIA.

Journal of Applied Polymer Science, Vol. 86, 1497–1506 (2002)

PLA–clay nanocomposites have special importance because of the promising properties of the polymer matrix and the possibility of high property enhancements by filling with nanoparticles. PLA–clay systems have already been prepared by the solution mixing and casting methods,[13] and these have shown improved mechanical properties, even if the filler, arranged in the form of tactoids consisting of several silicate monolayers, did not lead to a real nanocomposite (neither intercalation nor exfoliation). In this study, we prepared PLA–clay compositions by melt blending the components at an elevated temperature. Through this method, PLA-based nanocomposites loaded with 3 wt % organomodified montmorillonite (based on the inorganic content) and PLA-based microcomposites loaded with 3 wt % Na–montmorillonite were prepared. For the sake of comparison, unfilled PLA was processed under the same conditions. The work was focused primarily on the investigation of the structure and thermal behavior of PLA–montmorillonite nanocomposites compared to unfilled PLA and PLA-based microcomposites of a similar level of filling. We studied the crystalline and supermolecular structures of these systems by changing the processing conditions (isothermal crystallization and annealing from the solid amorphous state). Structural characterizations were carried out with different techniques: X-ray diffraction (XRD), light microscopy (LM), and size exclusion chromatography (SEC). The thermal behavior was determined with differential scanning calorimetry (DSC) and thermogravimetric analysis (TGA).

EXPERIMENTAL

Materials

PLA from Dow-Cargill, Inc. [Minnetonka, MN; weight-average molecular weight (M_w) = 166,000 and weight-average molecular weight/number-average molecular weight (M_w/M_n) = 2.0, as communicated by the producer] was used as the matrix. This polymer contains 4.1 mol % D-lactide and a residual lactide content of 0.27%.

Two clays, provided by Southern Clay Products (Gonzales, TX) were used in this study. Cloisite Na is a purified Na^+ montmorillonite clay with a cation exchange capacity of 92 mequiv/100 g. It is composed of stacks of silicate layers that are 0.96 nm thick and 250–500 nm wide with an interlayer distance of 1.22 nm.

A montmorillonite organically modified with dimethyl 2-ethylhexyl (hydrogenated tallowalkyl) ammonium cation was used to produce the PLA/clay nanocomposite. This modified clay contains 26–27 wt % of organic materials. It is characterized by a layer thickness equal to 0.96 nm and an interlayer distance of 2.07 nm.

TABLE I
Description of Investigated Samples

Material	Sample
PLA + 3 wt % organomodified clay	NC(Q)
	NC(A)
	NC(C)
PLA + 3 wt % Na^+ montmorillonite	MC(Q)
	MC(A)
	MC(C)
Unfilled PLA	PLA(Q)
	PLA(A)
	PLA(C)

Sample preparation

Before processing, PLA was dried at 105°C for 4 h under reduced pressure and then stored in the presence of a humidity absorbent. The blending of PLA with clay particles was conducted in the presence of 0.3 wt % Ultranox 626 stabilizer (General Electric Co., Parksburg, WV) on a counterrotating mixer (Brabender OHG, Duisburg, Germany) with a rotation speed of 60 rpm for 10 min. The processing temperature was set at 180°C; however, it rapidly increased to about 195°C on mixing. Compositions with 3 wt % (relative to the inorganic content) organomodified montmorillonite [nanocomposite (NC)] and with 3 wt % of Na^+ montmorillonite [microcomposite (MC)] were compounded. Unfilled PLA was prepared as well, with the same processing history. From these materials, 0.5 mm thick samples were prepared by compression molding at 185°C. Solidification was performed in air until the ambient temperature was reached. These conditions led to the quenching of the polymer. Two additional sets of samples were prepared first by annealing of the quenched sample at 120°C and second by crystallization from the melt at 120°C. Samples studied in this work are specified in Table I.

Instrumentation

PLA-based composites and unfilled PLA were characterized by several techniques. Thermal stability was assessed for quenched samples with TGA carried out on a Hi-Res TGA 2950 from TA Instruments (Brussels). Measurements were performed under thermooxidation and thermodegradation conditions, that is, under air and helium flow, respectively. The heating rate was 20°C/min. Thermal behavior was measured with a DSC 2920 from TA Instruments (New Castle, DE), with a heating and cooling ramp of 10°C/min under a nitrogen flow. The crystalline structure was measured by XRD analysis. The intensity of the X-ray distribution was measured at ambient temperature from 1.5 to 30° of 2θ with a scanning rate of 2°/min on a Siemens D5000 diffractometer (Karlsruhe, Germany) with Cu Kα radiation at λ = 0.15406 nm.

The supermolecular structure was examined for 50 μm thick films by means of a polarized light microscope (Polish Optical Works, Warsaw) equipped with Linkam hot stage (THMS 600, Epsom, UK). Samples were prepared between glass slides with analogous thermal conditions to those used for the preparation of the compression-molded samples. Molecular weight determination was carried out on all melt-processed samples. All the samples were dissolved in chloroform and filtered to eliminate the clay when present. Residual catalyst was removed by liquid–liquid extraction with a 0.1*M* HCl aqueous solution, and PLA was recovered by precipitation of the chloroform solution from cold methanol at 4°C. SEC measurements were carried out in tetrahydrofuran (THF; sample concentration = 2 wt %) at 35°C with a Polymer Laboratory (PL) liquid chromatograph (Hearlen, the Netherlands) equipped with a PL-DG802 degazer, an isocratic HPLC pump (LC1120, PL; flow rate = 1 mL/min), a Basic-Marathon autosampler from PL, a PL-RI refractive index detector , and four columns: a PLgel 10-μm guard column (50 × 7.5 mm) and three PLgel 10-μm mixed-B columns (300 × 7.5 mm). Molecular weights and molecular weight distributions were calculated by reference to a PS standard calibration curve, with the Kuhn–Mark–Houwink equation for poly (L-lactide) in THF: M_n (PLA) = 0.4055 × M_n (PS)$^{1.0486}$.[14]

RESULTS AND DISCUSSION

All the studied composites were obtained by melt processing. Both fillers, Na^+ montmorillonite and the organomodified clay, were readily incorporated in the melted PLA matrix. Visual examination of the quenched samples showed some opacity for the composite obtained with Na^+ montmorillonite, whereas the composites based on the organomodified clay and unfilled PLA were more transparent. As the polymer matrices of these samples could be considered amorphous by their thermal histories (and, therefore, transparent), the opacity of the Na^+ montmorillonite-filled composite may have resulted from the light scattering on the filler particles with their size comparable with the light wavelength. In turn, the transparency of the other composites suggests good dispersion of nanoclay particles within the polymer matrices without noticeable agglomeration in areas of size comparable with the wavelength of light.

XRD analysis

Figure 1 shows the XRD intensity distributions recorded for powders of Na^+ montmorillonite and organomodified montmorillonite (nanoclay) and for the quenched samples of unfilled polylactide [PLA(Q)], microcomposite [MC(Q)], and nanocomposite [NC(Q)]. PLA(Q) was characterized by a broad intensity maximum appearing approximately at $2\theta = 17°$, indicating an amorphous structure for this sample. As previously indicated, the visual opacity of MC(Q) and its observation by optical microscopy (vide infra) attested to the formation of a microcomposite. However, the XRD pattern of MC(Q) did not show any peaks corresponding to either the Na* montmorillonite or a possible intercalation [Fig. 1(d)]. The tiny content in Na^+ montmorillonite (3 wt %) dispersed in the PLA matrix might have been responsible for this observation. Indeed, already for Na^+ montmorillonite alone, the XRD pattern displayed a weak peak around 7.5° [Fig. 1(a)]. Therefore, this weak intensity peak was more likely buried under the very broad signal associated with the polyester matrix [compare Figs. 1(d) and 1(e)]. As far

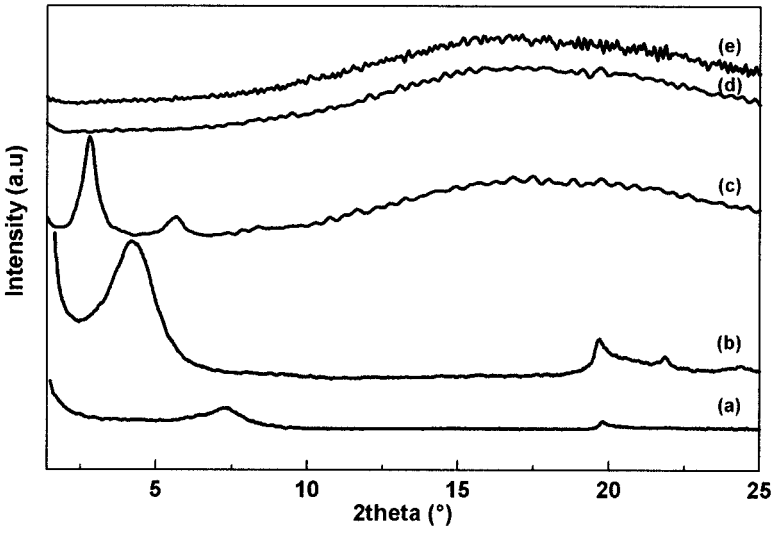

Figure 1 X-ray intensity distributions for (a) Na^+ montmorillonite powder, (b) organomodified montmorillonite, (c) PLA-based nanocomposite NC(Q), (d) PLA-based microcomposite MC(Q), and (e) unfilled PLA(Q).

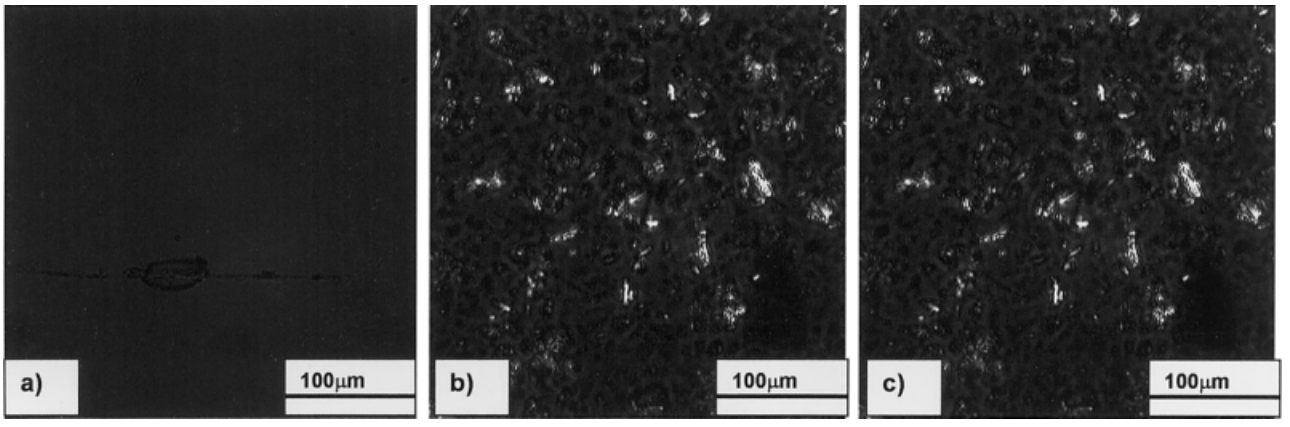

Figure 2 Polarized light micrographs of quenched samples taken at ambient temperature: (a) unfilled PLA(Q), (b) PLA-based microcomposite MC(Q), and (c) PLA-based molten microcomposite MC(Q) at 180°C.

as the organomodified clay was concerned, a distinct intensity maximum at 4.20° related to the (001) crystalline plane was detected, corresponding to an interlayer spacing of 21.0 Å. The nanocomposite exhibited two diffraction peaks at 2.80° corresponding to an interlayer spacing of 31.4 Å, and a secondary registry, (d_{002}), at 5.68°. An increase in the interlayer spacing from 21.0 Å in the nanoclay filler to 31.4 Å in the PLA nanocomposite gave credit to some intercalation occurring during the component blending above the melting temperature of the polymer matrix. This finding showed the possibility of penetration of the PLA chains within the nanoclay galleries on shearing at high temperature. Such an intercalation was not observed in the solvent-casting procedure.[13]

Polarized LM

Polarized LM pictures recorded at ambient temperature for quenched samples [unfilled PLA(Q) and MC(Q)] are presented in Figures 2(a) and 2(b), respectively. The LM pictures were completely dark for the PLA(Q) and NC(Q) samples [NC(Q) is not shown here], as they were practically amorphous according to the XRD and DSC results (vide infra). The PLA matrix of the MC(Q) sample was also amorphous. Therefore, the small bright regions seen in the pattern of this microcomposite [Fig. 2(b)] were due to depolarization and scattering of the polarized light by the microclay inclusions. This assertion was further confirmed as the same pattern was also observed for the molten microcomposite at 180°C [Fig. 2(c)]. Nanoclay inclusions (typically, primary particles composed of stacks of 20–40 intercalated clay sheets) were too small to be distinguished in the nanocomposite by the polarizing LM technique. On heating the quenched structure of the unfilled PLA and PLA composites, matrices underwent reorganization both on the crystalline and supermolecular levels. The latter event is shown in Figure 3(a–c) for samples annealed at 120°C for 1 h from the quenched state [PLA(A), MC(A), and NC(A) in Table I]. Microscopy images for these samples revealed crystalline aggregations seen as bright regions due to optical birefringence. They are characteristic for a thin spherulitic structure.[15] More details

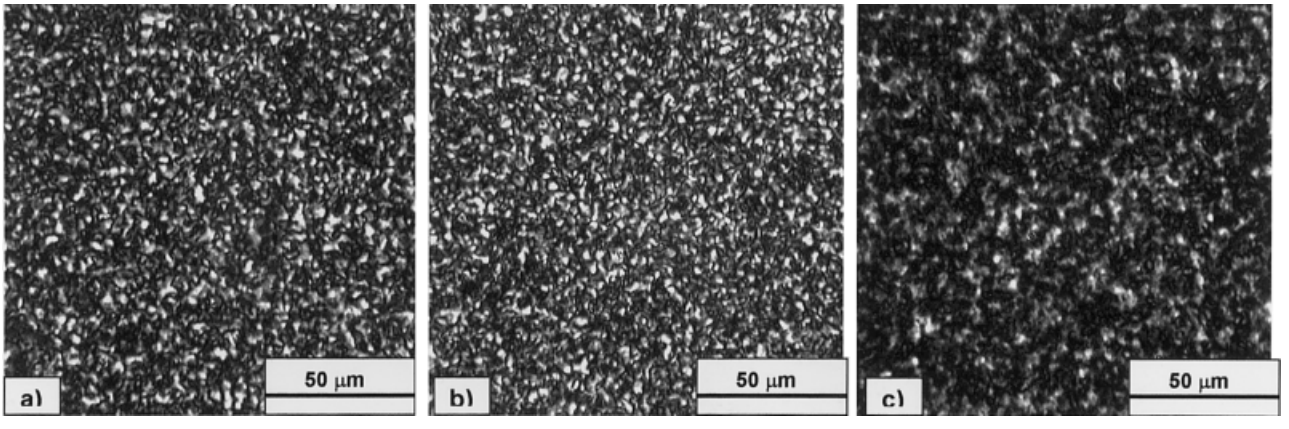

Figure 3 Polarized light micrographs taken at ambient temperature for samples annealed at 120°C from the quenched state: (a) unfilled PLA(A), (b) PLA-based microcomposite MC(A), and (c) PLA-based nanocomposite NC(A).

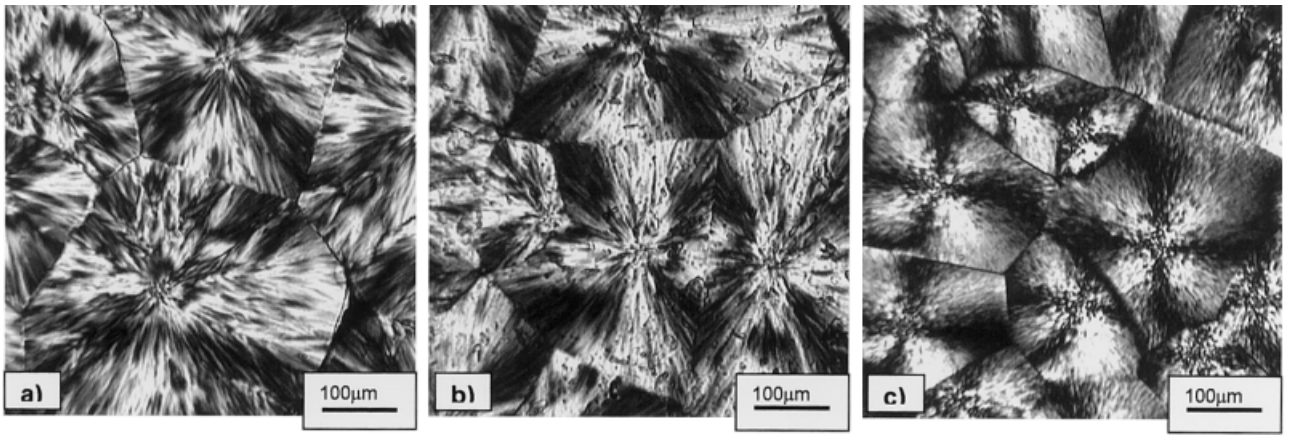

Figure 4 Polarized light micrographs taken at ambient temperature for samples crystallized at 120°C from the molten state: (a) unfilled PLA(C), (b) PLA-based microcomposite MC(C), and (c) PLA-based nanocomposite NC(C).

concerning structural alternations on heat treatment of the PLA were given in another article.[15]

Figure 4(a–c) shows images for PLA(C), MC(C), and NC(C) samples, respectively, prepared by isothermal crystallization at 120°C for 3 h from the molten state. Clearly, one can see that the overall morphology was influenced by the nature of the filler. The unfilled PLA(C) sample revealed well-developed spherulitic structure with a maximal size of spherulites around 330 μm. The spherulitic structure was also developed in both PLA/clay systems. However, the size of the largest spherulites decreased to about 200 μm in the microcomposite and to about 150 μm in the nanocomposite. This indicated some nucleation role of the filler toward the PLA matrix according to the observation that higher the number of inclusions was, the higher the number of spherulites was. One can also observe [Fig. 4(b,c)] that the growth of the spherulite front was not disturbed noticeably by the clay inclusions. As seen in Figure 4(b), the microclay inclusions were absorbed by spherulites. Therefore, one could expect that the microinclusions in the microcomposite and the nanoinclusions in the nanocomposite were incorporated into the interlamellar and/or intralamellar regions. The size and dispersion of the inclusion affected lamellar arrangement : it was coarse in the case of the microcomposite [Fig. 4(b)] and finer in the case of the nanocomposite [Fig. 4(c)].

DSC

DSC analysis was used to investigate both the glass-transition and crystallization/melting phenomena of PLA and PLA/clay composites in relation to the composition and preparation method. To illustrate that cooling at ambient temperature led to the quenching of the molten samples, we recorded DSC thermograms at a cooling rate of 10°C/min, which was of the same order as the cooling rate experienced by the compression-molded samples PLA(Q), MC(Q), and NC(Q), at least at the highest temperatures. The DSC cooling thermograms for unfilled PLA, microcomposite, and nanocomposite are presented in Figure 5(a). The thermograms did not reveal any crystallization exotherms; the jump in the heat flow observed below 50°C was attributed to the glass transition. The heating thermograms (at 10°C/min) recorded on the quenched samples displayed successively the glass-transition temperature (T_g), the cold crystallization exotherm with its maximum at T_c (the temperature of the cold crystallization maximum), and the melting endotherm at T_m [the melting temperature; Fig. 5(b) and Table II]. In-depth analysis of these thermograms revealed a sharp endothermic peak associated to the glass transition, typically attributed to stress relaxation on heating. The T_g values were practically independent of the sample composition. However, effects occurring at higher temperatures clearly depended on the sample composition. The ability to recrystallize decreased in filled PLA. The smaller the inclusions were, the more pronounced was the effect. Both the onset temperature of cold crystallization (T_1) and T_c increased going from PLA(C) to MC(C) to NC(C). On the opposite side, the heat of cold crystallization (ΔH_c) for these samples and, consequently, their respective heat of melting (ΔH_m) decreased in the same order (Table II). These data indicate that the nanomorphology present in the nanocomposite reduced noticeably the crystallization ability of the polymer. The ΔH_c and ΔH_m values for the respective samples were the same within experimental accuracy. Because the cold crystallization process is a time-dependent phenomenon, additional DSC measurements were performed for the quenched samples after an annealing at 120°C. Figure 6 presents the DSC heating thermograms for the annealed samples: unfilled PLA(A), PLA-based microcomposite MC(A), and PLA-based nanocomposite NC(A), respectively. The glass transition was observed as a weak jump on

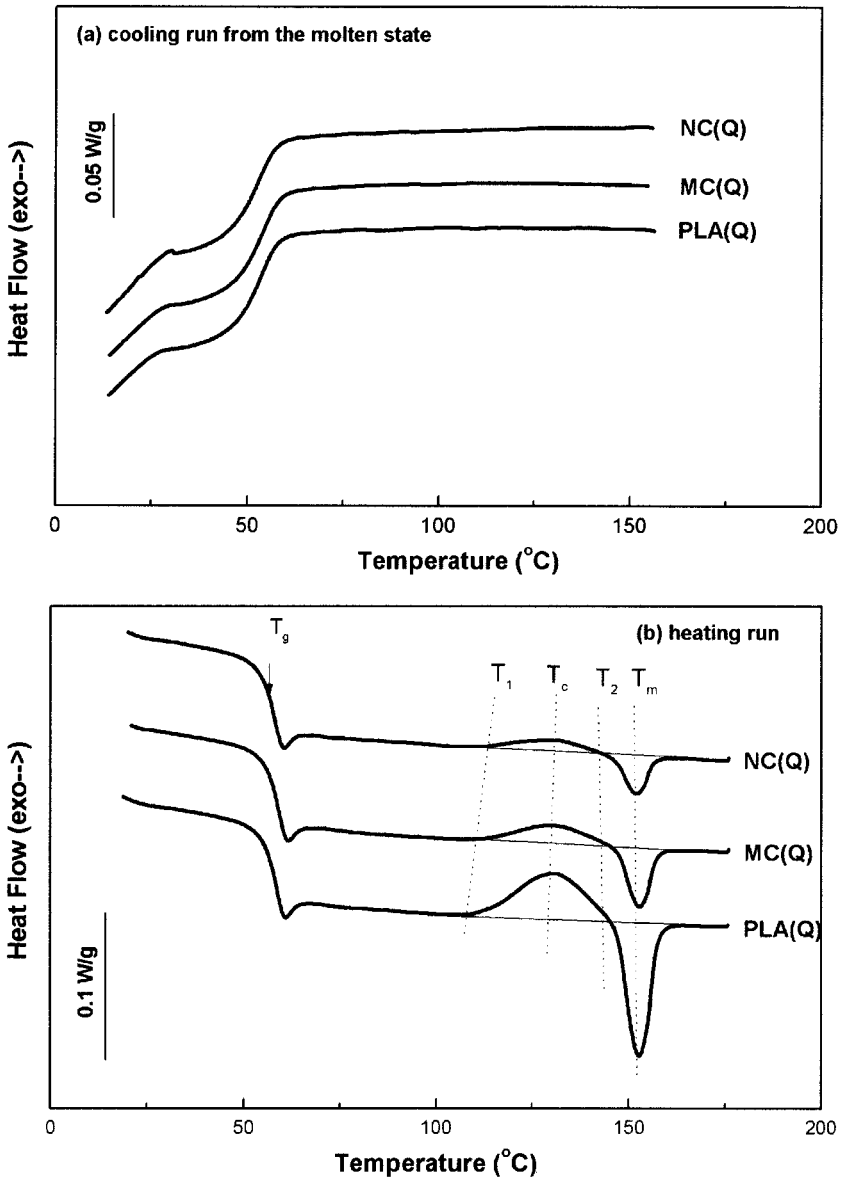

Figure 5 (a) DSC cooling thermograms recorded at −10°C/min from the molten state for unfilled PLA(Q), microcomposite MC(Q), and nanocomposite NC(Q) (this cooling rate led to quenching of the molten polymer) and (b) DSC heating thermograms recorded at 10°C/min for quenched unfilled PLA(Q), microcomposite MC(Q), and nanocomposite NC(Q) (T_2 = the onset temperature of the melting endotherm).

the heat flow curve without an endothermic maximum, as previously observed for the quenched samples. The T_g value remained unaffected by an annealing, and it was close to those recorded for the respective quenched samples (Tables II and III). All annealed samples exhibited one endothermic peak maximum;

TABLE II
Calorimetric Data Derived from the Second Heating Scan (10°C/min), Performed Immediately After Cooling from the Melt (10°C/min)

		Cold crystallization effects			Melting effects		
Sample	T_g (°C)	T_1 (°C)	T_c (°C)	ΔH_c (J/g_{PLA})	T_2 (°C)	T_m (°C)	ΔH_m (J/g_{PLA})
PLA(Q)	58.4	108.3	129.6	3.6	145.6	152.7	3.7
MC(Q)	58.5	110.6	130.0	1.6	144.5	152.8	1.6
NC(Q)	58.0	113.7	130.9	1.0	143.3	152.1	1.0

T_2 = onset temperature of the melting endotherm.

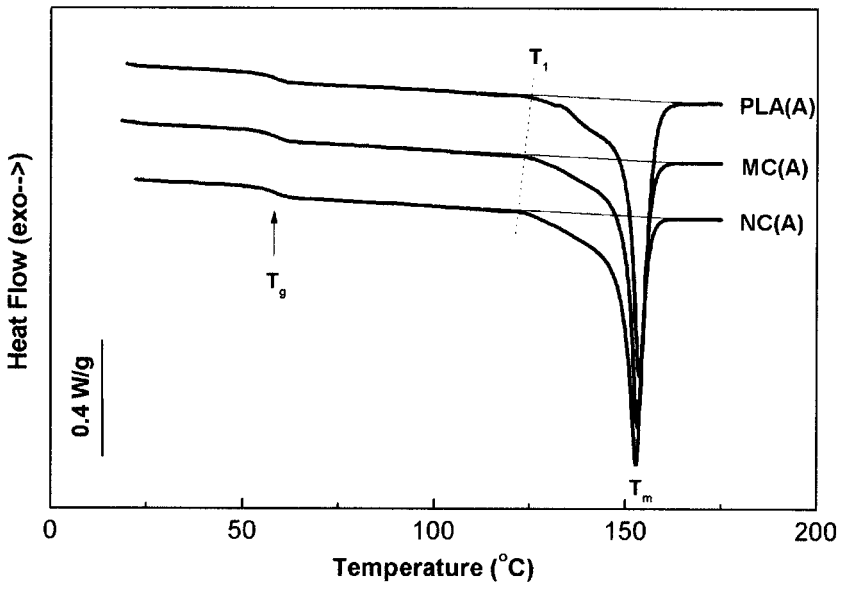

Figure 6 DSC heating thermograms recorded at 10°C/min for the samples annealed at 120°C from the solid amorphous state: unfilled PLA(A), MC(A), and NC(A).

T_1, T_m, and melting enthalpy (ΔH_m) appeared to be reduced for filled PLA, with a more pronounced effect in case of the nanocomposite. This observation again proved that the composite morphology affected the crystallization ability, even on annealing. In turn, Figure 7 displays the DSC heating thermograms measured for samples isothermally crystallized at 120°C from the melt, denoted as PLA(C), MC(C), and NC(C). The T_g, T_1, T_m, and ΔH_m parameters are collected in Table IV. The crystallized samples were characterized by the same T_1 and T_m values, indicating similar thermal stabilities of the crystalline elements in the samples despite different compositions. However, the ΔH_m value, corresponding to the relative content in crystalline phase, was significantly lower for filled PLA and, again, was smaller for the nanocomposite than for microcomposite (Table IV). Contrary to the quenched and annealed samples, the samples obtained by crystallization featured different T_g values. As the measurements were performed exactly within the same conditions (i.e., recorded at the same given time period after samples processing), the time factor could be neglected. Although unfilled PLA(C) exhibited the lower T_g, this transition increased from MC(C) to NC(C) (Table IV). A similar increase in T_g value was already reported for other intercalated nanocomposites, such as PS nanocomposites.[16] This behavior has been ascribed to the restricted segmental motions at the organic–inorganic interface neighborhood of intercalated compositions. However, in this work, the nature of tie molecules between crystallites should have also played a role, as some increase in T_g value was observed for MC(C), in which a phase-separated structure was formed.

TABLE III
Calorimetric Data Derived from the Thermograms (10°C/min) Obtained During Heating for Samples Previously Annealed at 120°C for 1 h

Sample	T_g (°C)	T_1 (°C)	T_m (°C)	ΔH_m (J/g_{PLA})
PLA(A)	58.4	125.4	153.7	42.3
MC(A)	58.8	124.3	153.1	39.5
NC(A)	58.2	121.9	152.7	38.7

SEC

PLA is known to rapidly degrade when melted at high temperatures, losing from 20 to 80% of its initial M_n on melt processing.[17] It was, therefore, interesting to compare the effect of filler incorporation on the evolution of M_n with thermal treatment. Table V shows the molecular parameters of both the native PLA and unfilled PLA(Q) and MC(Q) and NC(Q) after extraction of residual catalyst and clay when present.

As expected, PLA degraded on melt processing, even if a stabilizer (Ultranox 626) was added. A decrease in M_n of 41.2% was observed for unfilled PLA compared to the native PLA. However, even if the morphology arising from the clay dispersion (nanocomposite or microcomposite) did not appear to play some role, interestingly, the addition of either Na^+ montmorillonite or the organomodified clay strongly limited this degradation to only 22.1 or 19.6%, respectively. This molecular stabilization of PLA chains by the layered silicate filler clearly deserves more investigation and will be the topic of a forthcoming article.

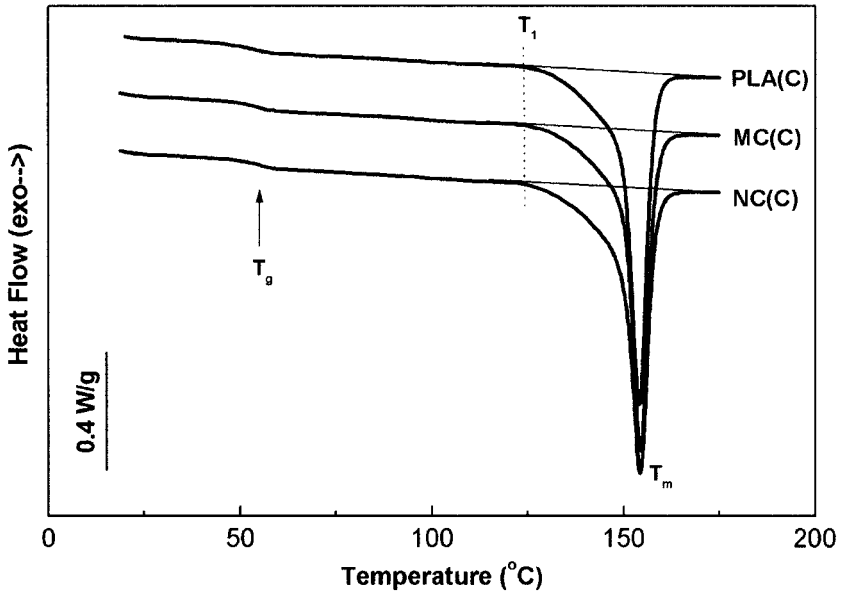

Figure 7 DSC heating thermograms recorded at 10°C/min for the samples isothermally crystallized at 120°C from the molten state: unfilled PLA(C), MC(C), and NC(C).

TGA and thermal stability

Thermal stability measurements were performed for quenched samples. One could expect that these results are also representative for samples prepared by annealing or isothermal crystallization from the melt. First, the burning behavior of the various samples were visually observed. Compared to both the unfilled PLA and the microcomposite, the nanocomposite burned in air without producing burning droplets. Instead, charring occurred that produced a solid black residue. This is a common behavior observed for nanocomposites and is partly responsible for their usually improved flame-retardant properties.[11,12] Figure 8(a) shows the TGA traces and their derivatives [differential thermogravimetry (DTG)] for unfilled PLA, the PLA microcomposite, and the PLA nanocomposite as obtained under an air flow. Figure 8(b) presents the same temperature-dependent weight loss that was recorded under a helium flow. In both cases, Na^+ montmorillonite did not significantly affect the thermal degradation: the maximum of the DTG curve was observed at the same temperature for the matrix and for the microcomposite under air and was only slightly shifted toward higher temperature under non-oxidative conditions. This slight shift may have arisen from the higher M_n observed in case of microcomposite. The most striking effect was observed for the nanocomposite. Although under helium its degradation temperature (determined at the DTG maximum peak) was increased by about 9°C, under air the increase was as high as 23°C. In this case, the shift in thermal stability could not be attributed to the difference in M_n, as they were comparable for both the microcomposite and the nanocomposite. The difference in thermal stability must, therefore, have been due to the difference in morphology observed between MC(Q) and NC(Q). The significant increase in thermal stability for the nanocomposite under thermooxidative conditions suggests a change in the degradation mechanism. For example, the char formation in the nanocomposite may have led to a physical barrier between the polymer medium and the superficial zone where flame combustion occurs. Such an increase in thermal stability has also been reported in the case of other nanocomposites, for example, for

TABLE IV
Calorimetric Data Derived from the Heating Runs (10°C/min) for Samples Isothermally Crystallized at 120°C from the Melt

Sample	T_g (°C)	T_1	T_m	ΔH_m (J/g_{PLA})
PLA(C)	52.9	124.0	154.1	52.6
MC(C)	54.1	124.0	154.3	51.6
NC(C)	54.9	124.0	154.3	49.0

TABLE V
Molecular Parameters for the Native PLA, Processed Unfilled PLA, and the Microcomposite and Nanocomposite After Clay Extraction

Sample	M_n[a]	M_w[a]	M_w/M_n
Native PLA	62,900	113,000	1.80
PLA(Q)	37,000	64,000	1.73
MC(Q)	49,000	95,100	1.94
NC(Q)	50,600	98,200	1.94

[a] Calculated by reference to a PS standard calibration curve with the Kuhn–Mark–Houwink equation for PLA in THF: M_n (PLA) = 0.4055 × M_n (PS)$^{1.0486}$ (see ref. 14).

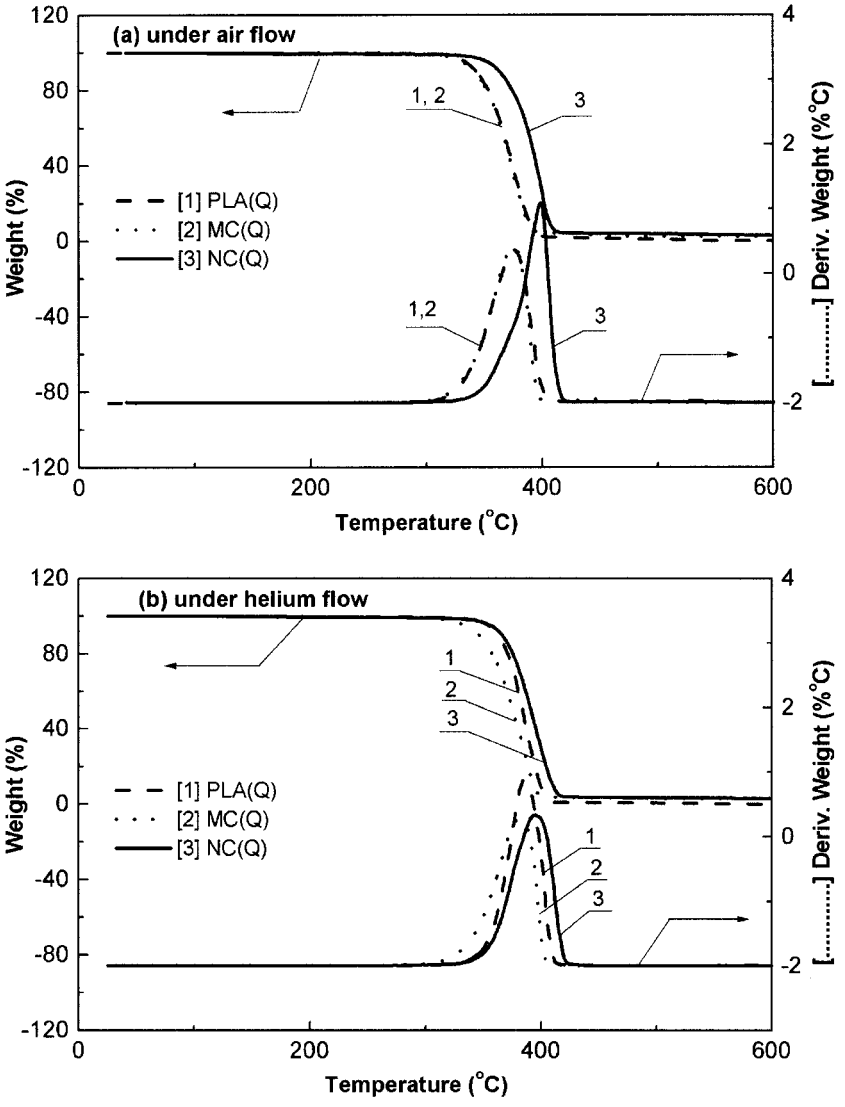

Figure 8 TGA and DTG traces recorded at 20°C/min under (a) air flow and (b) helium flow for (1) unfilled PLA(Q), (2) microcomposite MC(Q), and (3) nanocomposite NC(Q).

melt-blended EVA–montmorillonite nanocomposites exhibiting semi-intercalated semi-exfoliated structure[11] and intercalated nanocomposites prepared by emulsion polymerization of methyl methacrylate,[18] styrene,[17] or exfoliated crosslinked poly(dimethylsiloxane).[19] In every case, a high increase in thermal stability was observed, even at very low levels of filling.

CONCLUSIONS

Three PLA samples were prepared by melt blending in the presence of an antioxidant: unfilled PLA, a PLA/clay microcomposite, and a PLA/clay nanocomposite with the same amount of inorganics (3 wt %). In addition, different thermal histories were applied to the samples that revealed the influence of the composition on the structure and properties of the resulting materials. It was shown that the PLA-based microcomposite formed a phase-separated microstructure. It appears that PLA is a polymer that readily interacts during melt blending with a montmorillonite organomodified with dimethyl 2-ethylhexyl (hydrogenated tallowalkyl) ammonium cation, leading to the formation of at least an intercalated structure. The processing properties of the nanocomposite were excellent and comparable to those of the microcomposite and unfilled PLA. Both types of clay showed a tendency to limit PLA degradation. Thermal investigations showed an improvement in the nanocomposite thermal stability under oxidative conditions in comparison to those for the microcomposite and unfilled PLA. A deeper investigation of the nanocomposite morphology (transmission electron microscopy and small-angle X-ray scattering) are currently under investigation; the influence of the

ammonium cation used and the nanoclay filler content are also being investigated. They will by the subject of a forthcoming article.

The authors gratefully acknowledge Cargill-Dow Polymers, LLC, for supplying PLA. The authors thank Professors A. Rulmont and C. Henrist from the General Chemistry and Physics Chemistry Department at the University of Liege (Belgium) for the XRD measurements. M. Pluta thanks the Belgian FNRS and PAN cooperation agreement for a grant covering his stays in Mons, Belgium.

References

1. Jacobsen, S.; Degée, P.; Fritz, H. G.; Dubois, P.; Jérôme, R. Polym Eng Sci 1999, 39, 1311.
2. (a) Kojima, Y.; Usuki, A.; Kawasumi, M.; Okada, A.; Kurauchi, T.; Kamigaito, O.; Kaji, K. J Polym Sci Part B: Polym Phys 1995, 33, 1039; (b) Hasegawa, N.; Kawasumi, M.; Kato, M.; Usuki, A.; Okada, A. J Appl Polym Sci 1998, 67, 87.
3. Liu, L.; Qi, Z.; Zhu; X. J Appl Polym Sci 1999, 71, 1133.
4. Ke, Y.; Long, C.; Qi, Z. J Appl Polym Sci 1999, 71, 1139.
5. Weimer, M. W.; Chen, H.; Giannelis, E. P.; Sogah, D. Y. J Am Chem Soc 1999, 121, 1615.
6. Kornmann, X.; Berglund, L. A.; Sterte, J.; Giannelis, E. P. Polym Eng Sci 1999, 38, 1351.
7. Tyan, H.-L.; Leu, C.-M.; Wei, K.-H. Chem Mater 2001, 13, 222.
8. Chen, T. K.; Tien, Y. I.; Wei, K. H. J Polym Sci Part A: Polym Chem 1999, 37, 2225.
9. Lee, D. C.; Jang, L. W. J Appl Polym Sci 1996, 61, 1117.
10. Vaia, R. A.; Vasudevan, S.; Krawiec, W.; Scanlon, L. G.; Giannelis, E. P. Adv Mater 1995, 2, 154.
11. Alexandre, M.; Beyer, G.; Henrist, C.; Cloots, R.; Rulmont, A.; Jérôme, R.; Dubois, P. Macromol Rapid Commun 2001, 22, 643.
12. Alexandre, M.; Dubois, P. Mater Sci Eng 2000, R28, 1.
13. Ogata, N.; Jimenez, G.; Kawai, H.; Ogihara, T. J Polym Sci Part B: Polym Phys 1997, 35, 389.
14. Degée, P.; Dubois, P.; Jérôme, R. Macromol Symp 1997, 123, 67.
15. Pluta, M.; Galeski, A. J Appl Polym Sci 2002.
16. Lee, D. C.; Noh, M. W. Polym Bull 1999, 42, 619.
17. Degée, P.; Dubois, P.; Jérôme, R. Macromol Chem Phys 1997, 198, 1985.
18. Lee, D. C.; Jang, L. W. J Appl Polym Sci 1996, 61, 1117.
19. Giannelis, E. P.; Burnside, S. D. Chem Mater 1995, 7, 1597.